RESEARCH ARTICLE | AUGUST 07 2023

Design of the Lanthanum hexaboride based plasma source for the large plasma device at UCLA \odot

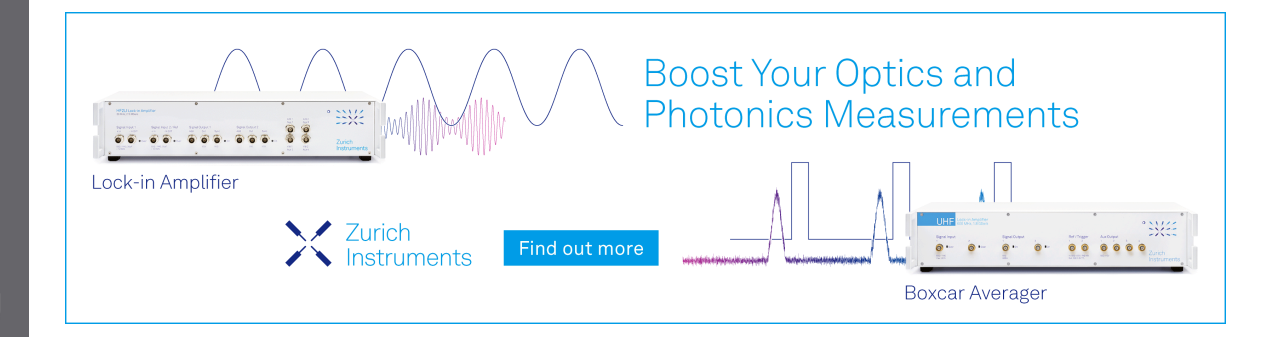
Yuchen Qian ■ (a); Walter Gekelman (b); Patrick Pribyl (b); Tom Sketchley; Shreekrishna Tripathi (b); Zoltan Lucky; Marvin Drandell; Stephen Vincena (b); Thomas Look (b); Phil Travis (b); Troy Carter (b); Gary Wan (b); Mattia Cattelan; Graeme Sabiston (b); Angelica Ottaviano (b); Richard Wirz (b)



Rev. Sci. Instrum. 94, 085104 (2023) https://doi.org/10.1063/5.0152216









Design of the Lanthanum hexaboride based plasma source for the large plasma device at UCLA

Cite as: Rev. Sci. Instrum. 94, 085104 (2023); doi: 10.1063/5.0152216

Submitted: 28 March 2023 • Accepted: 20 July 2023 •

Published Online: 7 August 2023







Yuchen Qian,^{1,a)} D Walter Gekelman,¹ D Patrick Pribyl,¹ D Tom Sketchley,¹ Shreekrishna Tripathi,¹ D Zoltan Lucky,¹ Marvin Drandell,¹ Stephen Vincena,¹ D Thomas Look,¹ D Phil Travis,¹ D Troy Carter,¹ D Gary Wan,² D Mattia Cattelan,³ Graeme Sabiston,² D Angelica Ottaviano,² D and Richard Wirz² D

AFFILIATIONS

- Department of Physics and Astronomy, University of California, Los Angeles, Los Angeles, California 90095, USA
- ²Department of Mechanical and Aerospace Engineering, University of California, Los Angeles, Los Angeles, California 90095, USA
- ³ Department of Chemical Sciences, University of Padova, 1-35131 Padova, Italy

ABSTRACT

The Large Plasma Device (LAPD) at UCLA (University of California, Los Angeles) produces an 18 m long, magnetized, quiescent, and uniform plasma at a high repetition rate to enable studies of fundamental plasma physics. Here, we report on a major upgrade to the LAPD plasma source that allows for more robust operation and significant expansion of achievable plasma parameters. The original plasma source made use of a heated barium oxide (BaO) coated nickel sheet as an electron emitter. This source had a number of drawbacks, including a limited range of plasma density (\lesssim 4.0 × 10¹² cm⁻³), a limited discharge duration (\sim 10 ms), and susceptibility to poisoning following oxygen exposure. The new plasma source utilizes a 38 cm diameter lanthanum hexaboride (LaB₆) cathode, which has a significantly higher emissivity, allowing for a much larger discharge power density, and is robust to exposure to air. Peak plasma density of up to 3.0×10^{13} cm⁻³³ in helium gas has been achieved. The typical operating pressure is \sim 10⁻⁵ Torr, while dynamic pressure can be achieved through the gas-puffing technique. Discharges as long as 70 ms have been produced, enabling a variety of long-time-scale studies of processes, such as turbulent particle transport. The new source has been in continuous operation for 14 months, having survived air leaks, power outages that led to rapid temperature changes on the cathode and heater, and planned machine openings. We describe the design, construction, and initial operation of this novel new large-area LaB₆ plasma source.

Published under an exclusive license by AIP Publishing. https://doi.org/10.1063/5.0152216

I. INTRODUCTION

Plasma sources capable of generating magnetized plasmas that are reproducible, quiescent, and spatially uniform at a high repetition rate (0.1–1 Hz) are highly desirable for studying fundamental plasma physics. The new large-area lanthanum hexaboride (LaB₆) cathode installed on the Large Plasma Device (LAPD) at UCLA (University of California, Los Angeles) achieves these properties while significantly improving operating capabilities over the previous barium oxide (BaO) source. This paper provides details of the design, construction, and initial operation of this new LaB₆ plasma source.

LaB₆ is known to have a low work function (about 2.6 eV) and high emission current density (>10 A/cm²), 2,3 making it a popular thermionic emitter. LaB₆ cathodes are commonly used as a discharge plasma source and are capable of producing plasmas with high electron densities (n_e > 10¹³ cm $^{-3}$). The new LAPD source features a 38 cm diameter LaB₆ cathode that is indirectly heated to ~1700 °C. The temperature uniformity of the LaB₆ cathode was optimized through a combination of thermal modeling and testing in order to generate the uniform electron emission current densities necessary for the production of a uniform plasma. The heater and cathode structure is designed to withstand thermal cycling and operational $\vec{J} \times \vec{B}$ forces, specifically pulsed discharge currents up to 10 kA in

a) Author to whom correspondence should be addressed: gianyuchen@ucla.edu

the presence of magnetic fields up to 0.8 T. The final cathode design has proven robust to both normal operation and off-normal events (e.g., rapid cooling during power outages).

The cathode is paired with a molybdenum mesh anode located 50 cm away; the pair is biased (~100 V) to create an electron beam, which ionizes and heats neutral gas (either static fill or gas puff). This produces an ~18 m long plasma column with a diameter of ~20 to 60 cm, depending upon the magnetic field configuration of the source and chamber. The vacuum pressure of the entire chamber is 5×10^{-7} Torrs, and a typical operating pressure is in the 10^{-5} Torrs range. The pressure can be dynamic with the gas-puffing technique. 4

This new LaB₆ cathode replaced a BaO based plasma source. The BaO cathode surface was made by spraying a uniform layer of a BaO mixture on a nickel sheet and heating it in vacuum to activate the coating. BaO is very sensitive to contamination (poisoning) and, thus, requires recoating whenever it is exposed to air, for instance, during scheduled maintenance or unscheduled vacuum leaks. The applied coating must be highly uniform in thickness; the electron emission profile, and hence the produced plasma profile, will reflect any nonuniformities in the coating. LaB₆, on the other hand, is more resistant to cathode poisoning and is capable of much higher electron emission current density. A variety of experiments were conducted in the plasma produced by this new cathode over the past year, proving that the design is durable and capable of generating reproducible, quiescent, and uniform plasmas. A photograph of the hot cathode and plasma is shown in Fig. 1

Considerable effort has been devoted to designing and testing prototype LaB $_6$ cathodes at the Basic Plasma Science Facility at UCLA. Several smaller cathodes have been used for a variety of experiments in LAPD. $^{6-10}$ The development of larger-scale designs started with a $20 \times 20 \, \mathrm{cm}^2$ square cathode source that was developed, installed, and operated in a low-magnetic field toroidal device. The design was then improved and made more robust for the higher current, higher magnetic field operation in LAPD. This resulted in the installation of a secondary plasma source (also a 20 cm square) in LAPD that was used as an auxiliary source in conjunction with the previous BaO cathode. This auxiliary source (which is still available for use with the new LaB $_6$ cathode) can be removed from the LAPD under vacuum to allow for alternative uses of the north end of the LAPD (e.g., injection of an intense ion beam 12). High density core plasmas, generated by the auxiliary source, embedded in lower

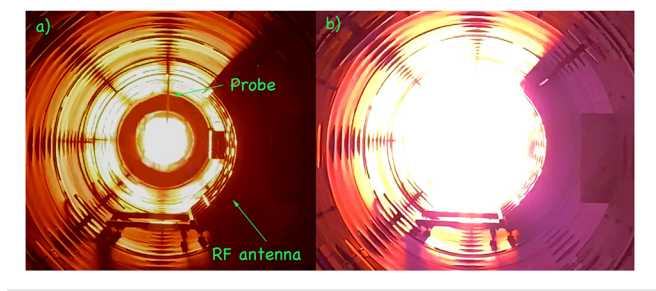


FIG. 1. (a) A view down the axis of LAPD before a plasma discharge. The cathode is the circular section at the center of the frame; the darker annulus around it is the end of the cathode chamber (smaller diameter than the main chamber). (b) Light from a He plasma axially filling the machine to a diameter of 60 cm.

density BaO-produced plasmas have enabled a number of important studies, including the realization of laser-driven collisionless shock formation $^{\!13}$ and excitation laser-driven shear Alfvén waves. $^{\!14}$ Lessons learned from the development of these cathodes were essential to the design, construction, and operation of the new 38 cm LaB6 primary source of the LAPD.

This paper is organized as follows: design details of the cathode and anode are presented in Sec. II, heater design is discussed in Sec. III, and the design of the enclosing chamber and shielding is discussed in Sec. IV. Performance of the LaB₆ cathode is evaluated in Sec. V based on COMSOL modeling, measurements, and user experience. Section VI shows examples of plasma parameters and profiles achieved with this new cathode. Section VII evaluates the overall performance of this upgrade and suggests future plans.

II. CATHODE AND ANODE

The cathode is a 38 cm diameter, 0.635 cm thick circular plate made of 99.5% pure sintered LaB₆ powder. In early tests, we found that using a single plate of this size invariably resulted in cracking due to the nonuniform thermal stress and deformation. Although small cracks do not affect the plasma, they typically grow until the cathode falls apart.³ Therefore, we cut the plate into four quarter-circle tiles to relax the thermal tension and allow small movements. The tiles are interlocked in a tongue and groove configuration [Fig. 2(c)] and embedded on a front panel with a circular opening that includes a "pocket" for the tiles on its periphery.

A carbon heater is located behind the LaB₆ cathode along with a thermally insulating enclosure to minimize the required heating power. The quarter-circle LaB₆ tiles are supported at their edges in the front panel of the cathode heater box. This panel is cut from a $61 \times 61 \times 1.27$ cm³ square carbon plate into a roughly octagonal shape with two side tabs. The carbon used throughout is POCO semiconductor graphite from Entegris, Inc. The surface as purchased or after machining is visibly smooth, not granular or porous.

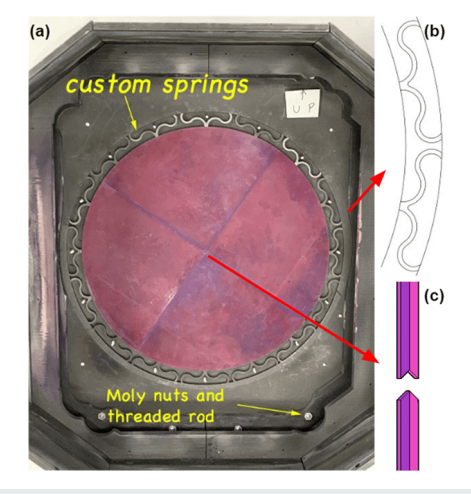


FIG. 2. (a) The backside of the LaB $_6$ cathode and front panel. (b) A detailed view of the carbon springs between the front panel pocket and the LaB $_6$. (c) A detailed view of the tongue-and-groove connection between the LaB $_6$ plate.

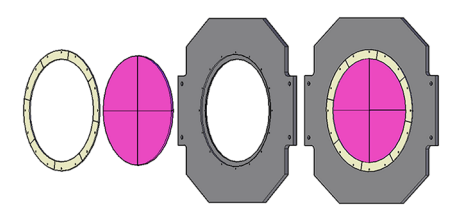


FIG. 3. An exploded (left) and assembled (right) CAD drawing of the front panel. Components from left to right are a carbon ring, LaB₆ plate, and the graphite panel.

The LaB₆ is held by a segmented ring affixed to the front panel by molybdenum bolts (Fig. 3).

Custom-made carbon springs press the tiles together from the side, ensuring a positive interlock for the tongue-and-groove joints between them [Fig. 2(a)]. The 16 mustache-shaped springs are equally spaced along the inner edge of the LaB₆ pocket. They hold the tiles in place along the circumference and at the same time allow radial expansions of about 2 mm. Their shape was computed to maximize stress uniformity throughout the length as they are deformed. In a previous design, zig-zag tantalum strips were used, but they became brittle during high temperature operation and needed frequent replacement. Figure 2(b) details the design of the springs, which were cut from a carbon block with electrical discharge machining (EDM).

The anode is a 64.4 cm diameter, 66% transparent molybdenum mesh, placed 50 cm away from the cathode. Different anode materials have been tested in the past: stainless steel lasted less than a week and copper sustained only one shot before melting. The anode is typically replaced at the same time as the cathode (14 months of operation for the most recent replacement). By this time, the initially ductile molybdenum had become brittle. The darkened central portion of the anode (Fig. 4), corresponding to the location of the plasma column, fractured under mild finger pressure.

A scanning electron microscope (SEM) was used to generate detailed images of the used anode. SEM micrographs show fuzz-like formation on the central portion of the anode, while evidence of blistering is observed in the outer ring. Energy-dispersive x-ray spectroscopy performed on the embrittled anode reveals significant amounts of carbon and chromium. It is suspected that carburization/decarburization contributes to the embrittlement of the anode 15,16 while the presence of chromium could indicate corrosion of stainless steel elsewhere in the machine. There is also evidence that the anode develops an insulating coating on the side facing the cathode. It is not known if the coating forms during normal operation—it may only become insulating after exposure to air. Investigations into embrittlement of the anode are ongoing and solutions to improve anode longevity, such as tungsten coating, are being explored.

The LaB_6 cathode temperature is maintained at a level to support stable plasma discharges by a heater that is run continuously.

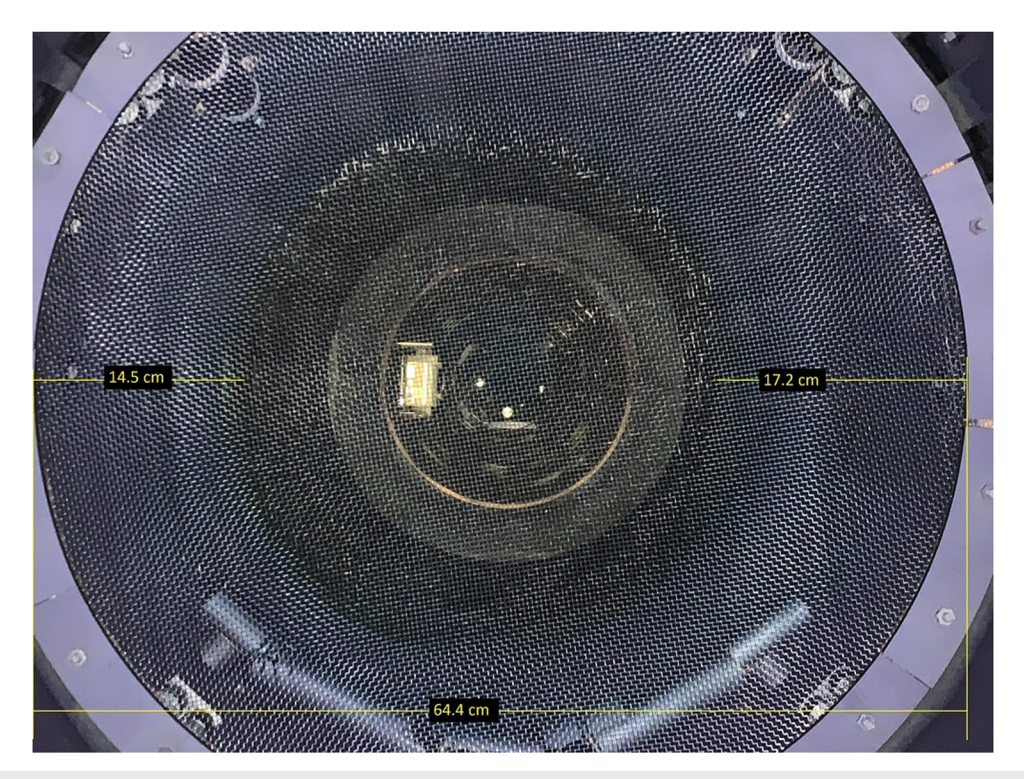


FIG. 4. Photo of the anode mesh after several months of operation. The circular burn mark in the middle shows the extent of the plasma column. The fact that it is offset seems to be reflected in plasma density profiles despite the apparent symmetry of the construction; the cause is still under investigation.

In this state, the cathode–anode voltage is pulsed to produce the plasma column. A discharge can be programmed to last between 10 and 70 ms, with a 0.1–1 Hz repetition rate. The discharge capacitor bank has a maximum voltage of 200 V and is typically charged to 80–170 V, depending upon the required density and temperature of a given experiment. Both cathode and anode are floating with respect to the chamber wall and connect to the wall through the plasma during the discharge. The anode potential generally has a 10–20 V difference relative to the wall.

Figure 5 explains the circuit connections of the LAPD cathode–anode pulser. Pulsed operation is controlled by the main transistor switch, made in-house with ten parallel insulated-gate bipolar transistors (IGBTs).¹⁷ An optional resistor may be connected across the main switch. With the resistor in the circuit, a 1–2 A

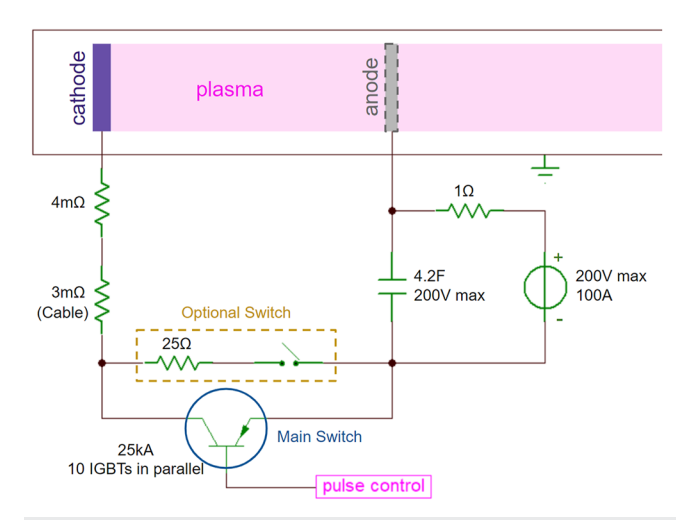


FIG. 5. Equivalent circuit of the cathode–anode in LAPD. The anode is biased positively by a variable power supply. The capacitor bank is 4.2 F and has a maximum voltage of 200 V. The main switch is a group of 10 IGBTs in parallel. The wall is grounded in most cases.

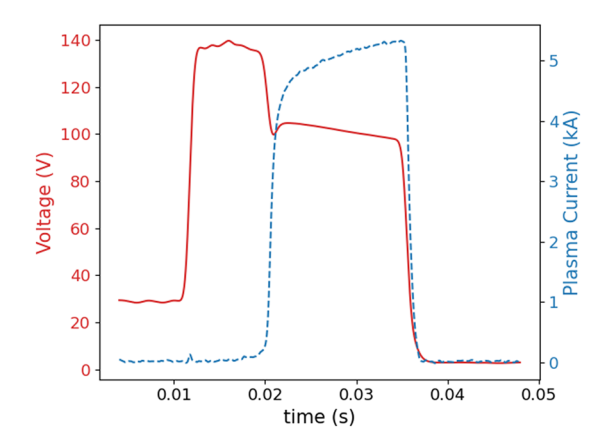


FIG. 6. The cathode—anode voltage (red solid line, axis on left) and plasma current (blue dashed line, axis on right) from a typical plasma discharge pulse.

plasma current is maintained between active-glow periods of the discharge to support smoother plasma breakdown.

A typical measurement of plasma current and cathode-anode voltage is shown in Fig. 6. The voltage is measured directly across the cathode and anode at the machine connections, and the plasma current is measured through a coaxial shunt resistor in series with the anode. In this specific experiment, the discharge capacitor bank was charged to 140 V and the optional resistor was included to generate a 1-2 A plasma to assist breakdown, seen as a ~30 V cathode-anode voltage before 10 ms. At ~10 ms, the IGBTs are switched on and a 140 V cathode-anode voltage develops. Between 10 and 20 ms, breakdown is achieved and the plasma discharge current grows exponentially. Meanwhile, the discharge current causes a voltage drop across the 4 m Ω resistor (and any series resistance in the cables/electronics), reducing the cathode-anode voltage and limiting the current growth rate. At 35 ms, the IGBTs shut off and residual plasma shorts the anode and cathode. The inter-pulse 30 V potential recovers 100-150 ms later (not shown).

III. HEATER

The heat source of the cathode is a specially designed array of POCO graphite serpentine heaters (Fig. 7). This array is located behind the LaB_6 cathode in a heat shielding enclosure, described later. A continuous 1.6–2.2 kA DC current is supplied for Joule heating the array. Heat transfer to the cathode is primarily through radiation.

The heater array has two parallel layers of graphite heater elements. Each layer has three serpentine heaters, or "snakes," which are all connected in parallel. Each snake consists of 13 horizontal rectangular bars (8.8 cm long \times 1.27 wide) with 14 annular sections (inner radius 1.778 cm, outer radius of 4.318 cm) connecting the rectangular bars in an alternating pattern. A tab (8.89 \times 2.54 cm²) at each end connects to either the current source or ground. A 0.445 cm thick carbon block is situated between the end tabs, connecting the two layers.

The serpentine design maximizes the radiation area facing the cathode while providing sufficient length for the total resistance to

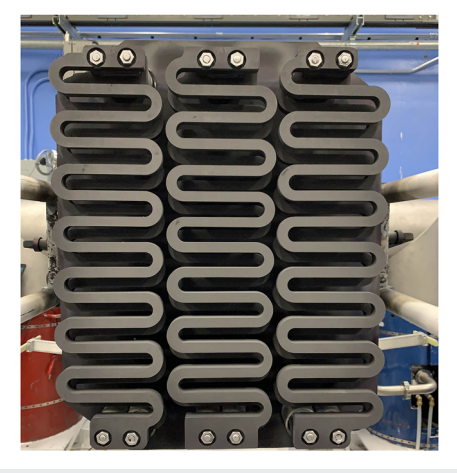


FIG. 7. Photo of the six serpentine heater elements, arranged in two layers.

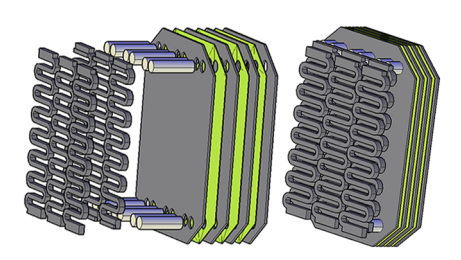


FIG. 8. An exploded (left) and assembled (right) CAD drawing of the heater and the heat reflectors. The heater has an offset between the two layers. The reflector includes four layers of carbon plate (colored black) and three layers of molybdenum sheet (colored green). The 12 white cylinders are boron nitride insulators over molybdenum conductors that feed the current to the heater elements; they also support the reflectors, with carbon washers as spacers.

match the output characteristics of the DC supply. The two middle snakes are $1.27\,\mathrm{cm}$ thick, while that outer four are $1.65\,\mathrm{cm}$ thick. This arrangement dissipates less heat in the middle snakes, resulting in a more uniform temperature profile across the emitting surface of the LaB₆. The two layers are offset by the width of one bar to optimize radiation efficiency.

The initial version of the heater used snakes that were 2.54 mm thinner than the current version. The thinner elements were plagued by carbon sublimation, leading to eventual heater failure. The sublimation rate increases by about an order of magnitude for every hundred degrees of temperature increase. Resistance also increases with temperature. If any section had a slightly elevated temperature, it would evaporate faster, becoming thinner. This would lead to more heating and, thus, faster evaporation. The problem was solved by increasing the carbon snake cross-sectional area. By providing more surface area, the same net resistive heating power could be radiated at a lower temperature. The increase over the original design lowered the temperature by an estimated 100°, and we have not had any noticeable evaporation with the thicker snakes.

Figure 8 illustrates how the heater is mounted to the other components. Cylindrical conductors enclosed in BN insulating tubes are molybdenum and provide a thermal interface between the hot elements of the heater and water cooled copper bus bars that eventually connect the heater current to outside the vacuum. An earlier design used uncooled copper for these cylinders, but they melted like wax candles.

IV. SHIELDING AND VACUUM CHAMBER

The heater assembly is enclosed in 0.762 cm thick POCO semiconductor graphite walls that prevent heat leaking from the side of the heater. The walls are screwed to the front panel using short molybdenum threaded rods with nuts. The back of the heater is covered by reflecting shields that are composed of alternate layers of carbon, tungsten, and molybdenum and held together by ceramic supports [Fig. 9(b)]. The walls and reflectors match the shape of the octagonal front panel. Together they form the heat shielding enclosure and are electrically isolated from the heater. Heater current conductors penetrate the rear of the reflectors through relatively small openings.

As described above, the LaB_6 cathode is in contact with the front panel; therefore, the entire heat shielding enclosure is at the

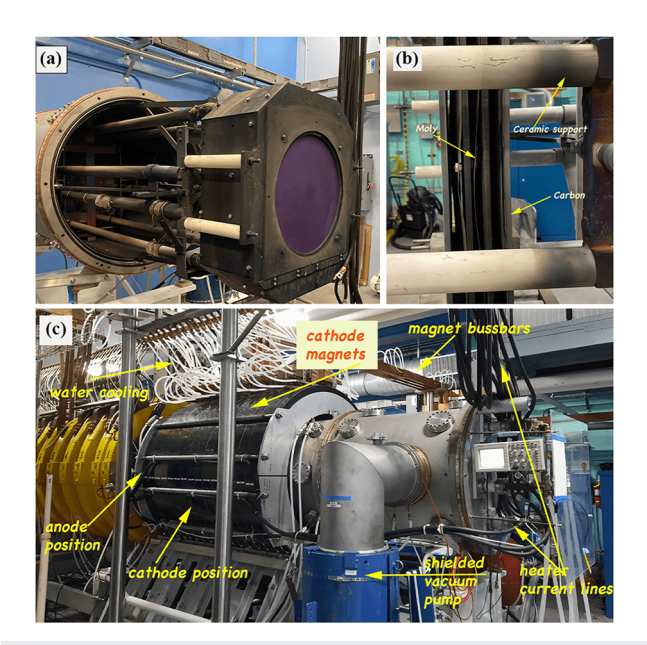


FIG. 9. (a) The cathode box mounted on the frame, taken out from the vacuum chamber. (b) The side view of the reflector assembly, placed behind the heater. (c) The vacuum chamber that houses the cathode and anode. It is attached to the yellow main LAPD chamber on the left.

cathode potential. Tabs on the front panel extend to either side, connecting to the plasma current feed conductors with molybdenum threaded rods. These current feeds also provide additional support for the front panel. The overall enclosure and current feeds are shown in Fig. 9(a).

The cathode and the anode are housed inside a 2 m long vacuum chamber, detachable from the main chamber [Fig. 9(c)]. It is surrounded by 16 electromagnets, powered independently from the magnets of the main chamber. The axial field in the cathode region can go as high as 8 kG. The chamber wall is cooled by water-cooled copper shrouds.

V. CATHODE PERFORMANCE AND SIMULATION

A COMSOL Multiphysics simulation was used to calculate the heat transfer, structural mechanics, radiation transfer, and electromagnetic effects of our system. The entire 3D cathode configuration, including the LaB₆, front panel and heat shielding enclosure, was considered. The 3D mesh geometries were constructed using COMSOL's built-in tool. The related parameters of the materials, such as emissivities, conductivities, and Young's modulus numbers, were taken from manufacturer reports and COMSOL's Material Library

The simulation was based on a typical operating condition of 2000 A heater current and 1 kG magnetic field that the assembly is immersed in. It assumed a vacuum environment. The generated plasma was not included in the simulations. Every design plan and its subsequent modifications were tested by COMSOL simulation, based on which the best design was chosen and sent for machining.

This paper only includes the simulation results of the design in use at the time of publishing.

The emission temperature for single crystal LaB₆ can range from 1027 to $1727\,^{\circ}$ C, 11,18 while the sintered LaB₆ powder needs a higher temperature. Previously published tests using a 30 mm diameter, 10 mm thick LaB₆ sintered powder disk show that it has the best emission for practical application above 1500 $^{\circ}$ C. 19 In our case, the LAPD cathode plate initiates stable plasma breakdown above $1620\,^{\circ}$ C. The manufacturer reports the melting point to be $2255\,^{\circ}$ C.

Figure 10 is a graph of the computed surface temperature on the emission side of LaB₆ at different operating currents. The model was compared and validated by measuring the cathode temperature using two dual-color infrared pyrometers: Omegascope OS3753 and Optris CTratio 2MH1. These pyrometers are mounted outside the vacuum chamber on a Pyrex viewport, and a mirror assembly is used to collect infrared radiation from the cathode. The measurement is averaged over 5×5 cm² in the middle of the cathode. At the typical operating current of 2000 A, the LaB₆ has a peak temperature around 1720 °C in the center region. The operation of the pyrometers depends on user provided emissivity and quotient of the emissivity of two infrared bands. These parameters were found from the literature.²⁰

Figure 11(a) shows the COMSOL calculation of the hot LaB_6 tiles in complete vacuum without the presence of the plasma. The simulation provides detailed information on the temperature distribution and temperature gradients, which is essential for iterations on the heater design and its improvement. The goal was to achieve the best spatial temperature uniformity at emission temperature.

A minimum temperature of $1620\,^{\circ}$ C in the center is necessary for practical emission from in-lab experience, although we generally do not raise the heater current to achieve a specified temperature since the emission of sintered LaB₆ depends on the manufacturing process. Instead, we adjust the heater current by as much as 10% around the typical 2000 A to produce desired plasma characteristics. In some target regimes, we reduce the temperature to produce higher voltage primary electrons, while in others, we increase the temperature to maximize emission current. The temperature gradient across the LaB₆ surface should be minimized to protect LaB₆ from local thermal stress that might lead to cracking. The construction of the LaB₆ and its support is highly constrained

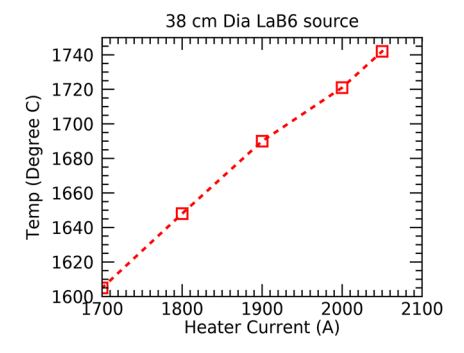


FIG. 10. The cathode surface temperature at different operating currents through the heater. The temperature is measured by a fiber based pyrometer focused at the center of the LaB $_6$ cathode, averaged over an area of 5 \times 5 cm 2 .

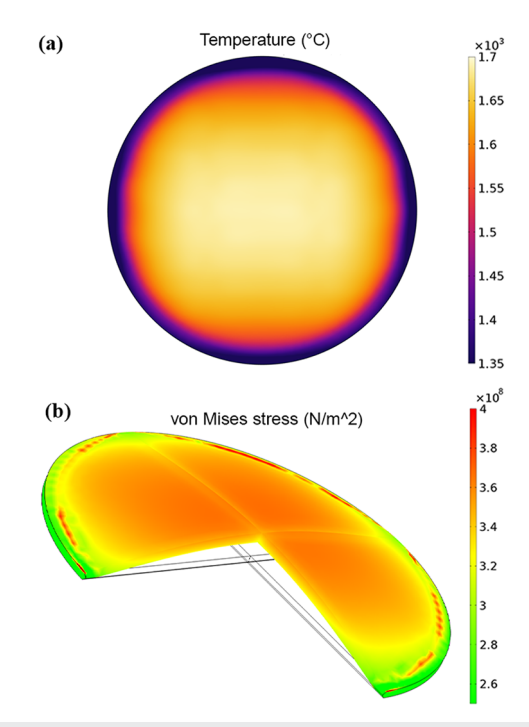


FIG. 11. COMSOL simulation of the (a) surface temperature and (b) von Mises stress on the LaB $_6$ tiles and its deformity in vacuum, with no plasma. The deformity is exaggerated for visible effect.

by manufacturing, and therefore, the heater layout is the major optimizable part in our design. Simulations were performed on several possible designs, and the calculated temperature distributions and material deformations were compared. Figure 11 shows the result from the final design at 2000 A.

When heated in vacuum, the center temperature was calculated to be around $1700\,^{\circ}$ C, with the edge cooling to $1550\,^{\circ}$ C. The low temperature around the edge is where the carbon ring (hidden from the picture) covers the tile and is not responsible for thermal emission.

After months of operation, the LaB₆ tiles slightly bulge toward the heater and away from the electron emission. An exaggerated view of the deformation is shown in the COMSOL simulation [Fig. 11(b)]. This is reasonable because there is a calculated temperature drop across the thickness of the cathode of up to 100 °C. The heater-facing surface is hotter, with correspondingly greater expansion, leading to the observed deformation. The calculated von Mises stress around the center, where the cathode withstands the largest plastic deformation, is roughly 36 MPa. COMSOL evaluates von Mises stress σ_{ν} using the calculated 3D stress tensor σ_{ij} : $\sigma_{\nu}^2 = \frac{1}{2} \left[\left(\sigma_{11} - \sigma_{22} \right)^2 + \left(\sigma_{22} - \sigma_{33} \right)^2 + \left(\sigma_{33} - \sigma_{11} \right)^2 + 6 \left(\sigma_{12}^2 + \sigma_{23}^2 + \sigma_{31}^2 \right) \right]$. This scalar is often used to predict deformation. The material starts yielding when σ_{ν} reaches a critical value.

The surface of the LaB₆ cathode is exposed to several materials inside the machine, including molybdenum from the anode mesh, carbon and tungsten from antennas and probes, corroded stainless steel from the machine wall, etc. It has been observed by J. Pelletier

and C. Pomot that poisoning from molybdenum will raise the work function of LaB₆ from 2.36 to 2.7 eV, 21 making the thermionic emission less efficient. The evaporated carbon also coats the backside of the LaB₆ after a long time of operation and modifies the heating. Therefore, it is necessary to frequently clean the cathode surface with hydrogen plasma and remove unwanted atoms.

Contamination and evolution of the surface have been studied for the ${\rm LaB_6}$ cathode at LAPD to further understand the cathode performance and lifetime.

SEM was used to generate detailed images of the fresh LaB_6 substrates from the manufacturer, as well as cathode samples after months of operation within the LAPD.

Figure 12(a) is of a fresh LaB₆ substrate. There are smooth areas of order 50 μ m on a side, which are interspersed with fissures showing crystalline material below. Figure 12(b) is from a sample exposed to, for the most part, He plasmas for several months. The discharge voltage varied from 60 to 90 V in these plasmas. The exposed surface became an irregular array of crystals, most likely due to ion bombardment. This structural change possibly reduced the lifetime of the sintered powder plate.

X-ray photoelectron spectroscopy (XPS) was also performed on the fresh and used LaB₆ substrates. Figure 13 shows the B 1s core level of a fresh LaB₆ substrate under different heating temperature.

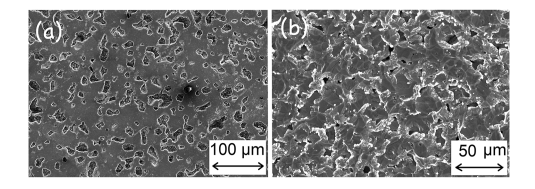


FIG. 12. SEM image of a piece of LaB $_{6}$ (a) before being installed in LAPD and (b) after several months of ion bombardment in, for the most part, a He plasma inside LAPD.

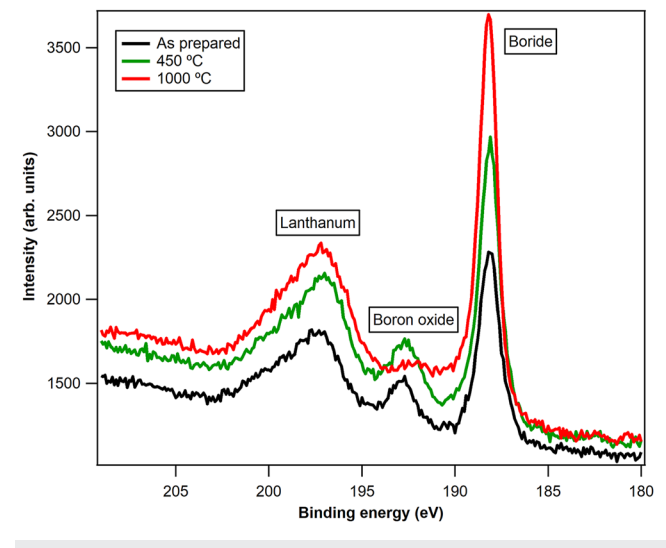


FIG. 13. XPS spectra of the B 1 s line using the fresh LaB $_6$ after different levels of heating under vacuum (8 \times 10⁻¹⁰ mbar).

We observe an initial proportion of the boron occurs at boron oxide, though it is removed via heating at 1000 °C.

A significant amount of carbon was observed on the surface of the fresh LaB₆ substrates, possibly from the handling and storage environment. The as-received LaB₆ was sent to be cleaned before being put into use. An even higher level of carbon was observed on the used LaB₆, likely from the evaporated graphite heaters, while the oxide levels found on the used LaB₆ were similar to the fresh sample. The carbon, along with oxide formation of the LaB₆, will cause the effective work function to be increased and hinder electron emission. Figure 13 indicates that heating to $1000\,^{\circ}\text{C}$ removed a noticeable amount of the carbon and oxygen, thus increasing the signal of B and La.

After running the system for months, several key elements of the operation have become apparent. The first is that the back of LaB $_6$ becomes coated with a layer of carbon with a thickness of 0.1 mm or greater.

This backside carbon layer does not seem to impact the operation. Second, once the cathode has been in operation for a period of months, exposure to air might result in the kind of cracks visible in Fig. 14. Close investigation shows a network of fractures that penetrate through or part way through the ceramic. Leaving a used cathode in the air for periods longer than a day results in progressive deterioration, until after a week it begins to completely fragment and fall apart. Interestingly, the deposited carbon layer on the back tends to maintain the overall integrity of the cathode material, although that also is not particularly robust to handling. We now use a positive pressure argon fill whenever maintenance (such as replacing a port) requires opening the machine. This has occurred four times with no detrimental effects to the cathode. These techniques have enabled the longest continuous use of a LaB₆ cathode to date, at 14 months as of the time of this writing. The cathode is continuously monitored with a camera that acquires and stores a high resolution photograph every few minutes. In spite of the machine opening and several rapid heater shutdowns (due to power glitches in the building). there are no visible cracks in the surface.

As mentioned in Sec. III, LaB₆ is always heated and the DC heater current is always on. The constant high temperature and currents on the heater are the cause for some difficulties. As the axial magnetic field is perpendicular to the plane of the heater current, the heater is under continuous a $\vec{J} \times \vec{B}$ force. Since the current flows in alternative directions in each bar of the snakes, the $\vec{J} \times \vec{B}$ force tends to split adjacent rectangular bars and, therefore, puts extra



FIG. 14. Cracked cathode.

tension on the semicircular bars. The force density per unit length is $\sim\!0.57$ MPa with 2000 A current at 1 kG axial field. This force is not significant compared to the mechanical stress. COMSOL computes the von Mises stress to be around 30 MPa on the semicircular bars. The POCO graphite is reported to have a comprehensive strength of 100 MPa and should not have a problem sustaining the tension. However, plastic deformation does occur, and without careful planning of the position and size of the heater components, the turn of the snake might expand and quickly touch the adjacent snake, causing a disastrous short. Another unexpected aspect of this design is that the hot carbon elements slowly deform over time. In initial realizations, they would eventually touch despite the initial clearance. We mitigate this by reversing the overall sense of the current on a monthly basis.

At the time of this writing, the cathode and springs had survived 14 months of continuous operation, often at high current ($I_D \geqslant 10$ kA). The LAPD was opened up, and the cathode and heater were in excellent condition. The difference in cathode thickness from center to edge was 1 mm. The heater thickness changed by less than 1 mm. The cathode, anode, and springs were replaced although they looked like they could last for another year.

VI. PLASMA AND EXPERIMENTS

Most of the experiments in LAPD happen at least 3 m away from the cathode-anode chamber, where the plasma can be highly quiescent. There are 450 access ports and 64 rectangular ports along the machine that allow two-dimensional freedom for probes and antennas. The current fed to the heater is typically 2000 A. The corresponding voltage drop across the heater is measured to be around 60 V.

Figure 15 shows a typical density profile, measured with the ion saturation current to a Langmuir probe, calibrated by a microwave interferometer. The probe is free to move across the cross-sectional plane. The data shown in Fig. 15 are recorded 703 cm away from the cathode and show good symmetry. The density reaches 8.0×10^{12} cm⁻³ at the center of the machine. In this case, the axial magnetic field was straight and the density profile maps to the cathode. When the magnetic field in the source is increased, the plasma column expands by the ratio $R_{\rm exp} = \sqrt{B_{source}/B_{0z}}$. Here, B_{0z} is the axial field in the bulk of the plasma in the main chamber and B_{source} is the field in the cathode chamber. With the appropriate magnetic field setup, the plasma column diameter in LAPD can expand up to 0.6 m.

Table I compares the capability of the old BaO cathode and the new LaB₆ cathode. The updated cathode clearly extends the variety of experimental environments that can be created in LAPD. The plasma parameters presented here were measured in the core region (r < 20 cm) of the plasma column in helium gas. The low range of the density was measured in plasma afterglow. Parameters for the BaO cathode were measured using Langmuir probes and interferometers and typically varied through power scans. For the LaB₆ cathode, Thompson scattering was added as a diagnostic, and the parameters are achieved by adjusting both power and fueling rate during gas puff operation. The ion temperature was measured using a He II line dispersed in a 1.3 m monochrometer with a 1200 l/mm grating.

Many topics in plasma physics can be studied within the LAPD plasma parameters, including energetic particle trapping, Alfvén

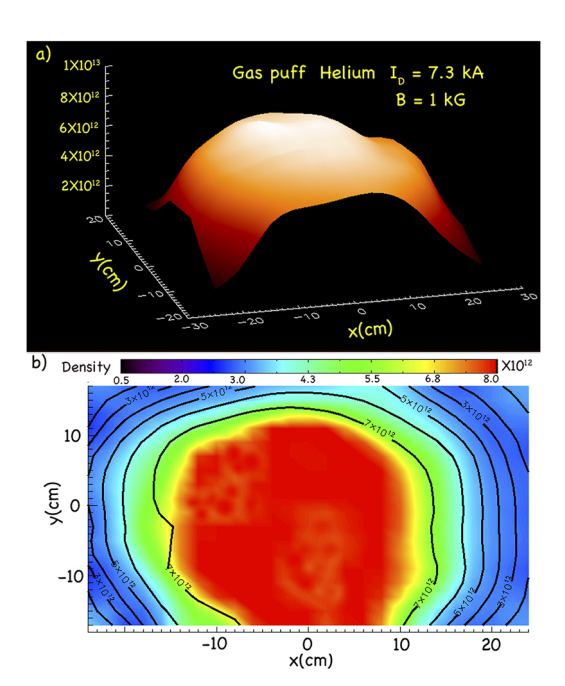


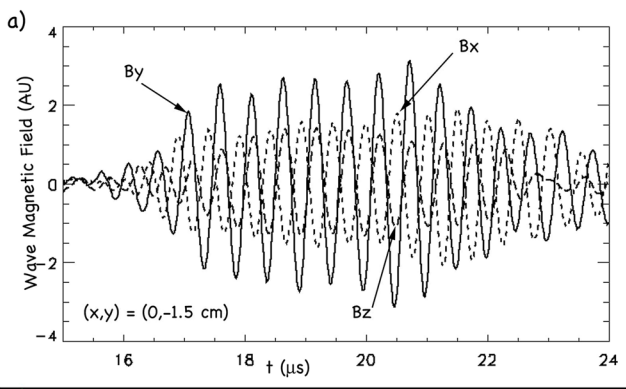
FIG. 15. (a) Shaded surface of the ion density in the LAPD device at 703 cm away from the cathode. The axial magnetic field is 1 kG and is straight throughout the machine. The helium feed-stock gas is puffed during the discharge. The plasma current is 7 kA with a discharge voltage of 135 V. (b) Contours of plasma density corresponding to the surface in (a).

TABLE I. Comparison of the typical range of basic plasma and operational parameters provided by the old BaO cathode and the new LaB_B cathode.

	BaO cathode	LaB ₆ cathode
Density (cm ⁻³)	$0.8 - 4.0 \times 10^{12}$	$0.02-3.0 \times 10^{13}$
Electron temperature (eV)	0.25 - 8.0	0.5-17
Ion temperature (eV)	0.5-1.5	0.5-9.0
Repetition rate (Hz)	1, 0.5, 0.25	0.1-1
Pulse duration (ms)	5–15	10-70

wave propagation, magnetic reconnection, flux rope studies, and filamentary structures, to name a few. The new LaB₆ cathode boosts the highest electron density from a scale of 10¹² to 10¹³ cm⁻³ and now allows the creation of hot ions, further expanding the possibilities. Experiments conducted after the new cathode installation include RF sheath rectification, turbulent blobs, fast wave excitation by fast ions, and Alfvén wave propagation.

For example, a fast Alfvén wave was launched 11.1 m from the cathode using a Rotating Magnetic Field (RMF) Antenna²² at $f = 5.0 \cdot f_{ci}$. The wave was detected with a three-axis magnetic probe 1.3 m away. The wave magnetic field on a plane is displayed in Fig. 16. The fast wave propagates along and across the field, and Figs. 16(a) and 16(c) show the components B_x , B_y , and B_z to be equal in magnitude, which is expected for a fast wave. Although the data plane in Fig. 16(b) was not large enough, it suggests that λ_{\perp} is of



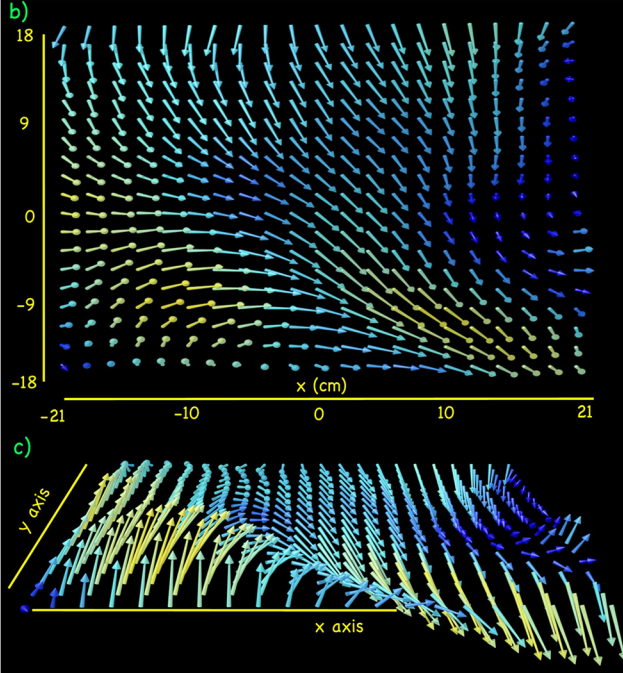


FIG. 16. (a) Temporal magnetic field of three components of an Alfv én wave launched at $f=5.0 \cdot f_{ci}$. The background magnetic field was 1 kG. The LAPD discharge current was 4.01 kA at 135 V. The detector probe and launch antenna were 1.3 m apart. (b) The vector magnetic field at one instant of time $t=17.72~\mu s$. (c) Alternate view, showing that the fast wave has a substantial z component.

order 50 cm. This is expected for a background magnetic field of 1 kG and a plasma density (measured with an interferometer) of 5.0×10^{12} cm⁻³.

With the lower density range provided by the old BaO cathode, λ_{\perp} will be in the range of a few meters, well beyond our data plane. In addition, in order to reach the large densities that are required for Alfvén wave studies, large discharge currents and voltages must be provided. The coating of the BaO cathode was rapidly destroyed by ion bombardment. The discharge pulse was limited to 10-15 ms to preserve the coating, while the LaB₆ cathode can sustain discharges of up to 70 ms, giving us greater freedom to customize the launching of the waves.

A host of future experiments, including magnetic field line reconnection, tearing mode, and ion and electron beam studies, to name a few, are in the planning stages.

VII. CONCLUSION AND FUTURE EXPERIMENTS

The new LaB₆ cathode in LAPD has shown its capability of producing a highly quiescent magnetized plasma that is 18 m long and 0.6 m in diameter. The electron density can be as high as 3.0×10^{13} cm⁻³ in a 1 kG axial magnetic field using helium gas. Electrons and ions can be consistently heated up to 17 and 9 eV, respectively. The ions are highly magnetized. At 1 kG, helium ions at 1 eV have a 0.4 cm gyroradius. The vacuum pressure of the chamber is 5×10^{-7} Torrs. While the operating pressure typically falls in the 10^{-5} Torrs range, it can be highly dynamic using gas-puffing. The range of plasma parameters is still expanding as we develop gas puffing and heating techniques on the LAPD.

The plasma is reproducible under a high repetition rate, and the cathode configuration can sustain long-time operation under high temperature and $\vec{J} \times \vec{B}$ force. The present cathode has been in continuous operation for 14 months with no sign of cracking or other damage. It has been vented to argon several times and undergone monthly thermal cycling when the heater leads were reversed. This is a substantial upgrade from the previous barium oxide based cathode, which only produced electron density up to $4.0 \times 10^{12} \, \mathrm{cm}^{-3}$ and required frequent re-coating. For BaO, cathode cleaning, re-coating, and heating to emission temperature without poisoning took about ten days.

With the new LaB $_6$ cathode installed, various physical processes can be studied within the plasma parameters. Experiments on topics such as energetic particle trapping, Alfvén wave propagation, and filamentary structures had been successfully performed in LAPD, while magnetic field line reconnection and ion and electron beam studies are on the schedule.

Further improvement on the cathode is on the plan to minimize the temperature gradient on LaB_6 and reduce deformation. Possible upgrades include optimization on the heater design and different geometry of the LaB_6 plate. More diagnostics, such as connecting thermocouples to the cathode structure, will be employed to accurately evaluate cathode performance.

ACKNOWLEDGMENTS

The authors thank the Department of Energy Office of Fusion Energy Science (Award No. DE-FC02-07ER54918) and the National Science Foundation (Award No. 1561912) for funding, which made this study and construction of the plasma source possible. We also thank Tai Ly and Avdit Kohli for their great technical support.

AUTHOR DECLARATIONS

Conflict of Interest

The authors have no conflicts to disclose.

Author Contributions

Yuchen Qian: Conceptualization (equal); Data curation (equal); Formal analysis (equal); Visualization (equal); Writing – original

draft (lead); Writing - review & editing (equal). Walter Gekelman: Conceptualization (equal); Data curation (equal); Formal analysis (equal); Funding acquisition (equal); Supervision (equal); Writing - original draft (equal); Writing - review & editing (equal). Patrick Pribyl: Conceptualization (equal); Data curation (equal); Formal analysis (equal); Visualization (equal); Writing original draft (equal); Writing - review & editing (equal). Tom Sketchley: Software (equal); Visualization (equal). Shreekrishna Tripathi: Data curation (equal); Formal analysis (equal); Writing - review & editing (equal). Zoltan Lucky: Conceptualization (equal); Project administration (equal); Supervision (equal); Validation (equal). Marvin Drandell: Project administration (equal). Stephen Vincena: Conceptualization (equal); Resources (equal); Validation (equal). Thomas Look: Data curation (equal); Formal analysis (equal); Writing - original draft (equal); Writing - review & editing (equal). Phil Travis: Data curation (equal); Formal analysis (equal). Troy Carter: Conceptualization (equal); Funding acquisition (equal); Project administration (equal); Supervision (equal); Validation (equal); Writing – review & editing (equal). Gary Wan: Data curation (equal); Formal analysis (equal); Writing - original draft (equal); Writing - review & editing (equal). Mattia Cattelan: Data curation (equal); Formal analysis (equal). Graeme Sabiston: Data curation (equal); Formal analysis (equal). Angelica Ottaviano: Data curation (equal); Formal analysis (equal). Richard Wirz: Data curation (equal); Supervision (equal).

DATA AVAILABILITY

The data that support the findings of this study are available from the corresponding author upon reasonable request.

REFERENCES

- ¹W. Gekelman, P. Pribyl, Z. Lucky, M. Drandell, D. Leneman, J. Maggs, S. Vincena, B. V. Van Compernolle, S. K. P. Tripathi, G. Morales, T. A. Carter, Y. Wang, and T. DeHaas, "The upgraded large plasma device, a machine for studying basic Frontier plasma physics," Rev. Sci. Instrum. 87, 025105 (2016).
- ² J. M. Lafferty, "Boride cathodes," J. Appl. Phys. **22**, 299 (1951).
- ³D. M. Goebel, Y. Hirooka, and T. A. Sketchley, "Large-area lanthanum hexaboride electron emitter," Rev. Sci. Instrum. **56**, 1717–1722 (1985).
- ⁴S. Tripathi, W. Gekelman, P. Pribyl, S. Vincena, and C. Niemann, "Uniform plasma produced using gas puffing in the Large Plasma Device at UCLA" (uppublished)
- ⁵D. Leneman, W. Gekelman, and J. Maggs, "The plasma source of the large plasma device at University of California, Los Angeles," Rev. Sci. Instrum. 77, 015108 (2006).

- ⁶D. Pace, M. Shi, J. Maggs, G. Morales, and T. Carter, "Exponential frequency spectrum and Lorentzian pulses in magnetized plasmas," Phys. Plasmas 15, 122304 (2008).
- ⁷S. Karbashewski, R. Sydora, B. B. Compernolle, and M. Poulos, "Driven thermal waves and determination of thermal conductivity in a magnetized plasma," Phys. Rev. E 98, 013204 (2018).
- ⁸B. V. Compernolle, M. Poulos, and G. J. Morales, "Sudden collapse of a pressure profile generated by off axis heating in a linear magnetized plasma," Phys. Plasmas **29**, 042104 (2022).
- ⁹W. Gekelman, E. Lawrence, and B. V. Van Compernolle, "Three-dimensional reconnection involving magnetic flux ropes," Astrophys. J. **753**, 131 (2012).
- ¹⁰B. V. Compernolle, J. Bortnik, P. Pribyl, W. Gekelman, M. Nakamoto, X. Tao, and R. Thorne, "Direct detection of resonant electron pitch angle scattering by whistler waves in a laboratory plasma," Phys. Rev. Lett. 112, 145006 (2014).
- ¹¹C. M. Cooper, W. Gekelman, P. Pribyl, and Z. Lucky, "A new large area lanthanum hexaboride plasma source," Rev. Sci. Instrum. 81, 083503 (2010).
- ¹²S. Tripathi, P. Pribyl, and W. Gekelman, "Development of a radio-frequency ion beam source for fast ion studies on the large plasma device," Rev. Sci. Instrum. **82**, 093501 (2011).
- ¹³C. Niemann, W. Gekelman, C. Constantin, E. Everson, D. Schaeffer, A. Bondarenko, S. Clark, D. Winske, S. Vincena, B. V. Van Compernolle, and P. Pribyl, "Observation of collisionless shocks in a large current-free laboratory plasma," Geophys. Res. Lett. 41, 7413, https://doi.org/10.1002/2014gl061820 (2014).
- ¹⁴M. VanZeeland, W. Gekelman, S. Vincena, and G. Dimonte, "Production of Alfvén waves by a rapidly expanding dense plasma," Phys. Rev. Lett. 87, 105001 (2001).
- ¹⁵K. Tsuya and N. Aritomi, "On the effects of vacuum annealing and carburizing on the ductility of coarse-grained molybdenum," J. Less-Common Met. **15**, 245–257 (1968).
- ¹⁶H.-P. Martinz and K. Prandini, "The carburization and nitriding of molybdenum and TZM," Int. J. Refract. Metals Hard Mater. 12, 179–186 (1993).
- ¹⁷P. Pribyl and W. Gekelman, "24 kA solid state switch for plasma discharge experiments," Rev. Sci. Instrum. 75, 669 (2004).
- ¹⁸ A. Bellucci, M. Mastellone, S. Orlando, M. Girolami, A. Generosi, B. Paci, P. Soltani, A. Mezzi, R. Polini, and D. Trucchi, "Lanthanum (oxy)boride thin films for thermionic emission applications," Appl. Surf. Sci. 479, 296–302 (2019).
- ¹⁹ A. Bellucci, M. Mastellone, M. Girolami, V. Serpente, E. Sani, D. Sciti, and D. Trucchi, "Thermionic emission measurement of sintered lanthanum hexaboride discs and modelling of their solar energy conversion performance," Ceram. Int. 47, 20736–20739 (2021).
- ²⁰ J. Kowalczyk, M. Hadmack, E. Szarmes, and J. Madey, "Emissivity of lanthanum hexaboride thermionic electron gun cathode," Int. J. Thermophys. 35, 1538–1544 (2014).
- ²¹ J. Pelletier and C. Pomot, "Work function of sintered lanthanum hexaboride," Appl. Phys. Lett. **34**, 249 (1979).
- ²²A. Gigliotti, W. Gekelman, P. Pribyl, S. Vincena, A. Karavaev, X. Shao, A. Sharma, and K. Papadopoulis, "Generation of polarized shear Alfvén waves by a rotating magnetic field source," Phys. Plasmas 16, 092106 (2009).